HAADF Imaging: An Effective Technique for the Study of Nonhomogeneous Nanostructures

P. Santiago,[1] L. Rendón,[1] C. Reza-San Germán,[1] and U. Pal[2,*]

[1] *Instituto de Física, Universidad Nacional Autónoma de México, Apartado postal 20-365, Mexico D.F., México*
[2] *Instituto de Física, Universidad Autónoma de Puebla, Apdo. Postal J-48, Puebla, Pue. 72570, México*

Atomic number contrast (*Z*-contrast) imaging using high-angle annular dark field (HAADF) detector, along with high resolution electron microscopy (HREM), is used to study the nanostructured metal, semiconductor, mixed oxide, and soft matter composites of inhomogeneous nature. A comparison between the HREM and HAADF images for the analysis of crystal structure, defects, and compositional inhomogenity in those nanostructures has been made. While the HREM technique is efficient in determining bulk crystallinity and defect structures, the HAADF imaging technique is superior in determining the surface inhomogenity, defect structures in the interior of the nanostructures, even at atomic resolution. The efficiency of the HAADF imaging technique in determining the surface inhomogenity and defect structures is demonstrated for the Au–Pt bimetallic clusters, CdSe nanofibers and nanowires, $Nb_{16}W_{18}O_{94}$ mixed oxide, and polystyrene-mormorillonite clay nanocomposites.

Keywords: HAADF Imaging, Nanostructure, Semiconductors, Soft Matter.

COMMUNICATION

Recent progress in nanofabrication techniques produced several interesting nanostructures of semiconductors and metals[1–4] with special physical and chemical characteristics.[5–7] However, the application potential of these tiny structures depends on the efficiency of controlling their size, shape, and composition. While the size and shape of semiconductor nanostructures define their use in optoelectronics and of metals in catalysis, their composition remains the main controlling parameter for any application. Traditionally, the composition of bulk materials was estimated by using conventional techniques like XRD, EDS, ICP, SIMS, and XPS; however, for nanostructures, the techniques are not very efficient.[8–10] Although the global composition of nanostructures is being evaluated through EELS and the local composition by HREM, none of the techniques are effective for the evaluation of composition inhomogenity in nanostructures at the atomic level. While the global composition of nanostructures is important for controlling their physical properties, like optical, electrical, mechanical, and optoelectronic properties, the surface composition at the atomic level is very important for their applications in chemical and electro-chemical catalysis to control their selectivity and efficiency.

Electron microscopy techniques such as HREM have been the primary technique used to characterize nanocrystals size and shape.[11,12] Though this technique allows us to analyze individual nanocrystals to obtain average size distribution, it is not easy to determine the precise shape and size of the nanocrystals because of nanocrystal movement under an electron beam and poor contrast near the surface of the nanocrystals.[8] Phase-contrast imaging in HREM relies on lattice fringes, which arise from the periodic structure of a crystal lattice. This periodicity is broken at the surface and nearby lattice defects, complicating image interpretation.

On the other hand, *Z*-contrast scanning transmission electron microscopy (STEM) using an HAADF (high-angle annular dark field) detector can provide highly detailed images of nanocrystal surfaces, 3D information, and mass contrast simultaneously. HAADF uses high-angle scattered electrons to obtain spatially resolved images which are able to show subtle details about the shape and compositional inhomogenity of nanocrystals with moderate precision. Electron scattered to high angles are predominantly incoherent, and the images formed using HAADF

*Author to whom correspondence should be addressed.

do not show the contrast changes associated with coherent scattering.[13,14] However, this high-angle scattering is associated with electron interaction close to the nucleus of the atoms which constitute the sample (Rutherford scattering). So, the scattering phenomenon is strongly dependent on the atomic number Z. At this level, it is possible to assure that, on the order of 1 nm, the STEM images formed with the HAADF detector are highly sensitive to changes in specimen composition, with the intensity varying monotonically with composition and specimen thickness. Otherwise, HAADF atomic resolution images have a more complicated dependence associated to the excitation of Bloch states and electron channeling.[15] However, 3D atomic resolution is possible if a sufficiently thin specimen zone is present.

Another characteristic of HAADF images is their changes in focus with depth. In such a case, the depth of focus can be maximized through the optical configuration of the microscope, using a small condenser aperture to minimize the convergence angle.

In this paper we present the HAADF and HREM study of inhomogeneous metal, semiconductor, mixed oxide, and soft matter nanostructures to evaluate the superficial and bulk inhomogenity in them. While the HREM technique revealed their crystalline quality, orientation, and crystalline defects, the HAADF technique revealed their compositional inhomogenity even in the form of their structural defects at the atomic level. Our results demonstrate clearly the striking difference in efficiency between HAADF imaging and conventional TEM techniques for the evaluation of compositional inhomogenity in metal, semiconductor, oxide, and soft matter nanostructures.

Bimetallic nanoclusters of Au–Pt in colloidal form were synthesized through simultaneous chemical reduction technique as described elsewhere.[16,17] Nonstoichiometric one-dimensional (1D) CdSe nanostructures were synthesized through a solvothermal technique as reported in our earlier works.[18,19] In a typical solvothermal growth, selenium powders and cadmium chloride with 15% excess of the stoichiometric ratio were reacted in a 100-ml round-bottom flux filled with 80 ml of ethylenediamine at 140 °C for 4 h without stirring. After the reaction products were cooled, they were filtered and washed several times by ethanol and water. For microscopic observations, the samples were dispersed in methanol, spread on carbon-coated microscopic copper grids, and dried in vacuum.

To acquire the structural and chemical information simultaneously at the atomic level, we used nanocrystalline $Nb_{16}W_{18}O_{94}$ to study through HAADF imaging. The $Nb_{16}W_{18}O_{94}$ sample was synthesized by Juárez et al.[20] through a solid-state reaction, mixing NbO_2 (200 mesh), Nb_2O_5 (99.9%), WO_2 (100 mesh), and WO_3 (99.95%) in stoichiometric proportion. Adding 4 mg of $HgCl_2$ as mineralizing agent, the mixture was ground by an agate mortar and heated at 1100 °C in an evacuated quartz tube for 4 days. The final product was powdered and placed on a lacey carbon support TEM grid for microscopic observations.

Soft matter composites were prepared using styrene (C_8H_8) and sodic mormorillonite clay through polymerization by the emulsion method. [2-(Acryloyloxy)ethyl]-trimethylammonium chloride (2AETMAC) was used as the cationic monomer. The intercalation of the clay with the cationic monomer was carried out for 24 h and then the modified clay was loaded into a reactor with the styrene at 70 °C in a N_2 atmosphere. The resultant latex was purified and directly loaded on to a carbon grid for microscopic observations without any additional treatment.

Electron microscopy was performed with a JEM 2010 FasTem microscope equipped with an STEM unit, HAADF, and bright field (BF) detectors. The resolution in HAADF/BF-STEM modes was of the order of 0.2 nm.

As the first example of the potentialities of HAADF detector imaging, we consider the small bimetallic Au–Pt nanoclusters of molar ratio 1/3. From the Figure 1, the inhomogeneous distribution of Pt is evident on the bimetallic nanoparticle surfaces. From conventional HREM images, it is possible to observe the highly defective nature of the bimetallic particles with a lattice parameter of 2.25 Å (Fig. 1a) corresponding to the (111) reflection of bimetallic $AuPt_3$ with a tetragonal structure (PDF chart 150043). Figure 1b shows a strain surface maple-like bimetallic nanoparticle. The surface morphology in these samples is not the typical one which corresponds to plane circular monometallic particles, with no strain on

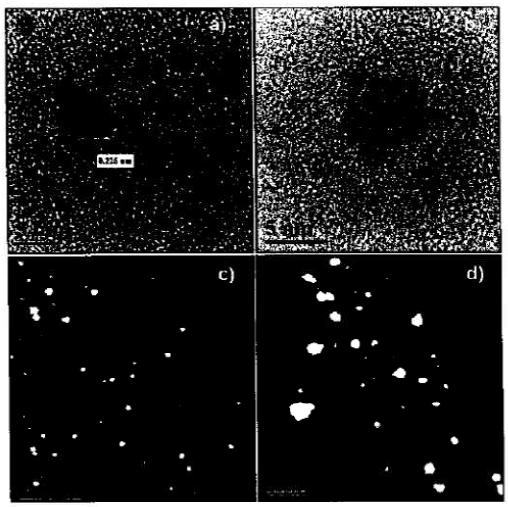

Fig. 1. HREM (a, b) and HAADF images (c, d) of Au-Pt bimetallic nanoparticles showing inhomogeneous elemental distribution. Au has a higher atomic number than Pt, therefore Au appears with brighter contrast. Inhomogencities at the surface of the bimetallic particle can also be observed through HAADF images (d).

the surface and minimum defects. Evidence of inhomogeneous distribution of elements is more palpable from the Z-contrast images (Fig. 1c, d), even though the difference in atomic number between the elements is very small. Very recently, Garcia-Gutierrez et al.[21] have shown the formation of core–shell structures in Pt–Au bimetallic clusters through HAADF imaging utilizing the strain field at the core–shell interface.

For CdSe 1D nanostructures, our solvothermal synthesis produced at least two different structures. The first one corresponds to CdSe nanofibers (NFs) of hexagonal phase[19] as shown in Figure 2. While from the low magnification image (Fig. 2a) it is clear that the NFs are generated from the stacking of CdSe layers of the hexagonal phase, the sensibility of the HAADF imaging technique to monitor the inhomogenity of the sample through mass contrast is visualized in Figures 2b, c. In fact, Figure 2c reveals many dark patches, which appear to be pores in the NFs but are really the crystallographic inhomogenity revealed by HAADF imaging. Through HREM, we could detect the formation of small grains of different crystallographic orientations embedded in the main growth layer (off-plane irregularities). The small grains are in different channeling condition to the electron beam with respect to the fibers, causing the contrast decay[22] and appearing as dark spot like contrasts in the images.

On the other hand, nanowires (NWs) of CdSe were also found in our samples. In Figure 3, the HREM and

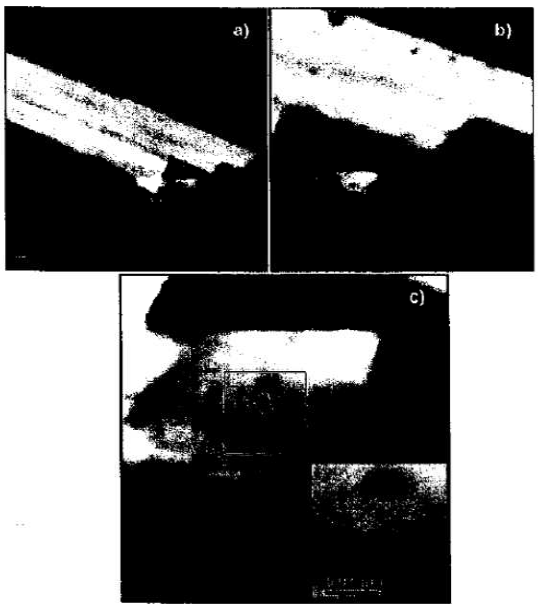

Fig. 2. (a) HAADF image from a hexagonal NF of CdSe. (b) A closer view shows the porosity in the NFs due to imperfect stacking of the CdSe layers. (c) High-resolution HAADF image shows the lattice fringes of the crystal (inset in c). The differences in density of the NFs are also evident.

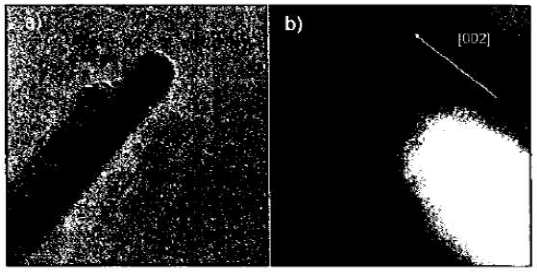

Fig. 3. (a) HRTEM image of a single-crystal CdSe NW with the FCC phase growing in the [002] direction. (b) HAADF image from the same single-crystal NW; the atomic columns are evident.

HAADF images of selected nanowires are presented. From the HREM image it is clear that CdSe NWs correspond to the FCC phase growing in the [002] direction. The lattice fringes are also evident in the HAADF image (Fig. 3b) only when the single crystal is well-oriented (channeling orientation). This is because in STEM mode, a convergent electron beam scans the surface of the sample, and high-angle dispersed electrons are collected by the annular aperture to generate the image. Therefore, the contrast of the atomic columns is obtained as a result of intensity integration during the illumination period. Since this type of scattering is incoherent, the intensity for each atomic column is independent of others. Consequently, the different species of atoms generate a different contrast in the image. In fact, these nonstoichiometric NWs are of core–shell type (Fig. 4). The core–shell structure is more evident in Figure 4b, where the Gatan image filter (GIF) is used around the Cd peak to locate the position of Cd in the nanostructures. We can observe that the excess Cd remains mainly at the surroundings of stoichiometric CdSe NW of the FCC structure. The bright contrast in the lattice columns also reveals the presence of Cd in the bulk of the NW structure.

The potentiality of the HAADF imaging technique in structure and chemical composition analysis of crystalline samples is more evident when we consider a complex oxide such as $Nb_{16}W_{18}O_{94}$. This sample is of special

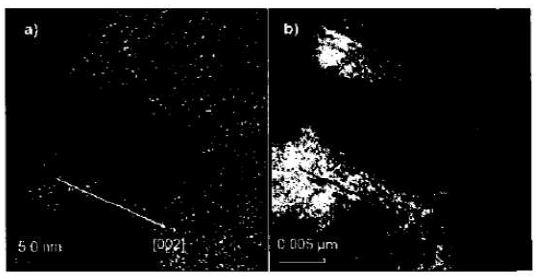

Fig. 4. Core–shell like CdSe nanowire of FCC structure: (a) HREM image and (b) Gatan image filter (GIF) image of the same NW showing a CdSe core surrounded by an amorphous Cd shell.

interest for HAADF study as it has large lattice parameters and is easy to orient using a double tilt sample holder.

High-resolution images acquired by the STEM technique using an HAADF detector are fundamentally obtained as the result of intensity integration over the illumination time. When an electron probe passes through the low-order orientation zone of a crystal, the atoms act like microlenses and focus the electron wave function.[21,22] The tendency of electrons to channel along the atom columns in crystals greatly increases its intensity due to the cooperative focusing effect. Therefore, the channeling effect has a great contribution on the STEM visibility of the atomic position in crystals.

Apart from that, HAADF imaging is effective for analyzing thicker samples. While conventional high-resolution TEM does not allow observation of high-resolution details (Fig. 5) of the sample due to thickness, the HAADF image of the same zone reveals the lattice fringes of the crystal at the same magnification. Generally, the small dependence of HAADF imaging on sample thickness allows us to analyze samples up to 50 nm thick.[22] Moreover, there is no contrast problem in HAADF images due to defocus conditions of the sample. The bright columns shown in Figure 5b correspond to the projected atomic columns, even when the thickness and defocus conditions do not allow observation of any structural information by conventional HRTEM. The intensities for the atomic columns are independent of each other, without interference of the electron waves. On the other hand, the channeling effect strongly depends on the orientation of the atoms with respect to the incident electron beam. In order to obtain a high-resolution HAADF (HR-HAADF) image, the sample must be tilted to a specific crystalline orientation and the channeling effect is improved by using a Ronchigram microdiffraction pattern.[23] Figure 6a shows a HR-HAADF image of a $Nb_{16}W_{18}O_{94}$ sample corresponding to the [001] zone axis. The corresponding FFT inverse processing image using CRISP[24] software is presented in Figure 6b with the unit cell marked. The unit cell projected along [001] is presented in Figure 6c where the blue,

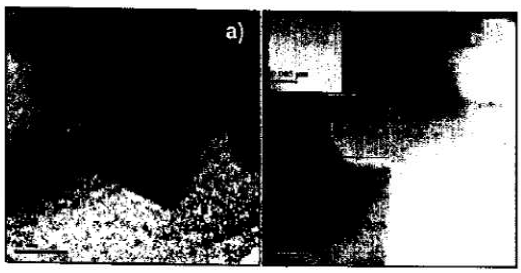

Fig. 5. Selected area image from $Nb_{16}W_{18}O_{94}$: (a) Conventional TEM image. Thickness of the sample does not allow observation of any details. In this case, the morphology of the zone is the only detail observed. (b) HAADF image from the same zone. The orientation of the sample allows observation of the channeling lattice image.

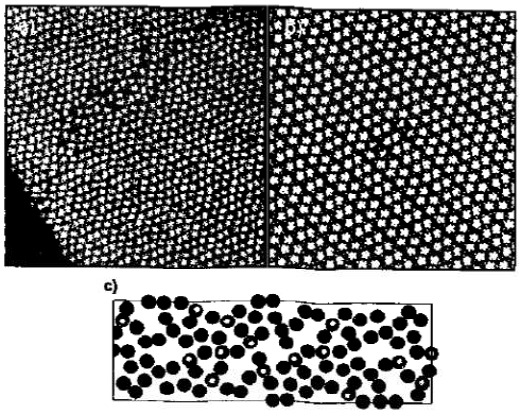

Fig. 6. (a) Atomic resolution HAADF image of $Nb_{16}W_{18}O_{94}$ crystal in the [001] direction. (b) CRISP processed image showing distinct contrasts for Nb, W, and O. The unit cell is marked. (c) Structural model of $Nb_{16}W_{18}O_{94}$ unit cell projected along the [001] direction.

green, and red balls represent W, Nb, and O atoms, respectively. In the Figure 6a, the darker contrast squares correspond to the segregated $WO_{2.90}$ of the monoclinic phase with interplanar spacing $d = 2.331$ nm in the (001) direction, which clearly shows the ability of the HAADF imaging technique for obtaining spatially resolved chemical analysis apart from the structural details of nanostructures.

The technique is also extremely useful for the studies of soft matter samples such as polymer composites and biological systems, conventionally prepared with a complex staining and embedding process for microscopic observations. Soft matter nanostructure samples can be observed with minimum damage using HAAF, as the current density of the focused electron beam (on the sample) can be minimized using a small spot size (0.5 nm) with an arrangement of very small condenser apertures (15 μm). As evidence, we analyzed styrene modified mormorillonite clay composites by HREM and HAADF imaging. In Figure 7a, a bright field STEM (BF-STEM) image of the sample is presented. The BF-STEM image is understood as equivalent to conventional transmission electron microscopy in terms of the reciprocity rule.[13] In fact, the BF detector does not exclude the coherent Bragg reflections, and therefore, the image is largely influenced by defocus, thickness, and diffraction contrast. The conventional HREM image does not reveal any significant contrast difference due to the presence of the mormorillonite clay in the composite, as there is no diffraction contrast or it is minimum. However, at the same magnification, the HAADF image (Fig. 7b) reveals the Z-contrast evidence of the presence of clay. From the image, it is clear that the clay forms a very thin layer covering the polystyrene balls inhomogeneously (white arrows in Fig. 7b). At higher magnification and using low dose in conventional HREM, the lattice fringes of the clay surrounding the styrene are

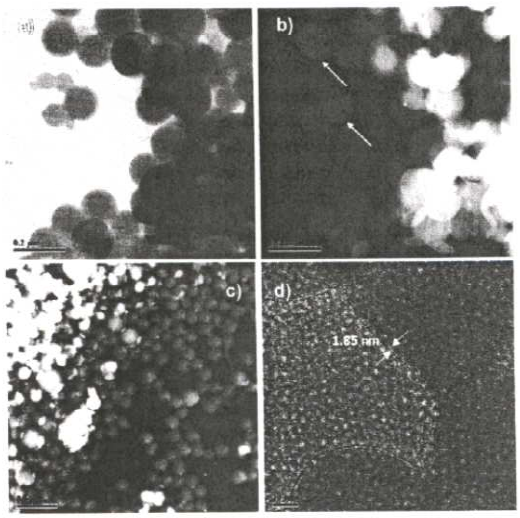

Fig. 7. (a) BF-STEM image from a styrene-modified sample with mormorillonite sodic clay. Almost no contrast differences between the styrene and clay are present. (b) HAADF image from the same zone. The brightness zone corresponds to the clay layer, while the styrene appears in dark contrast. (c) A HAADF general view. (d) HRTEM image where the lattice of the clay is clear. The clay is covering the styrene balls.

COMMUNICATION

observed (Fig. 7d). The lattice parameter is found to be of 1.85 nm instead of 1.7 nm, corresponding to the mormorillonite sodic clay as a result of lattice expansion produced during the monomer intercalation process. The obvious advantage of using the HAADF detector for TEM observations of polymers is that the sample does not have to be stained, a technique which modifies the real structure of the original material by introducing external crystalline material.

In conclusion, Z-contrast imaging using a HAADF detector shows great promise for characterizing metal, semiconductor, mixed oxide, and even soft matter composite nanostructures and biological samples. Apart from the high resolution, detailed chemical information related to the chemical/compositional inhomogenity obtained from this technique cannot be obtained using conventional TEM techniques using dark- or bright-field detectors. Additionally the technique is useful to detect local strain field[25,26] and location of composition-related defects, along with phase inhomogenity inside and outside the nanocrystal lattice.

Acknowledgments: This is due to PAPIIT-UNAM for financial support through the projects grants IN108303-3 and IX107204. We are thankful to Professor Carlos Guzman de las Casas for providing the polymer nanocomposites. We are also thankful to Central Microscopy facilities of Institute of Physics, UNAM, for providing the microscope facilities used in this work.

References and Notes

1. D. Xu, X. Shi, G. Guo, L. Gui, and Y. Tang, *J. Phys. Chem. B* 104, 5061 **(2004)**.
2. Z. Liu, Z. Hu, J. Liang, S. Li, Y. Yang, S. Peng, and Y. Qian, *Langmuir* 20, 214 **(2004)**.
3. B. P. Zhang, N. T. Binh, K. Wakatsuki, Y. Segura, Y. Kashiwaba, and K. Haga, *Nanotechnology* 15, S382 **(2004)**.
4. D. Yu and V. W. Yam, *J. Am. Chem. Soc.* 126, 13200 **(2004)**.
5. D. Cao and S. H. Bergens, *J. Power Sources* 134, 170 **(2004)**.
6. L. F. Dong, Z. L. Cui, and Z. K. Zhang, *Nanostruct. Mater.* 8, 815 **(1997)**.
7. D. L. Klein, R. Roth, A. K. L. Lim, A. P. Alivisatos, and P. L. McEuen, *Nature* 389, 669 **(1997)**.
8. J. R. McBride, T. C. Kippeny, S. J. Pennycook, and S. J. Rosenthal, *Nano Letters* 4, 1279 **(2004)**.
9. S. J. Pennycook and D. E. Jesson, *Ultramicroscopy* 37, 14 **(1991)**.
10. Y. Peng, P. D. Nellist, and S. J. Pennycook, *J. Electron Microsc.* 53, 257 **(2004)**.
11. J. J. Shiang, A. V. Kadavanich, R. K. Grubbs, and A. P. J. Alivisatos, *J. Phys. Chem.* 99, 17417 **(1995)**.
12. D. J. Smith, *Rep. Prog. Phys.* 60, 1513 **(1997)**.
13. A. Howie, *J. Microsc.* 177, 1 **(1997)**.
14. S. J. Pennycook, *Ultramicroscopy* 30, 58 **(1989)**.
15. R. F. Kirkland, J. Loane, and Silcox, *Ultramicroscopy* 23, 77 **(1987)**.
16. J. F. Sanchez-Ramirez, G. Diaz, A. Vazquez, and U. Pal, *J. New Mater. Electrochem. Appl.* (in press).
17. R. Esparza, J. A. Ascencio, G. Rosas, J. F. Sánchez Ramírez, U. Pal, and R. Pérez Campos, *J. Nanosci. Nanotechnol.* 5, 641 **(2005)**.
18. J. A. Ascencio, P. Santiago, L. Rendón, and U. Pal, *Appl. Phys. A* 78, 5 **(2004)**.
19. U. Pal, P. Santiago, J. Chavez, and J. A. Ascencio, *J. Nanosci. Nanotechnol.* 5, 609 **(2005)**.
20. I. Juárez, *Electrochemical Intercalation of Lithium into the Solid Solution* $Nb_{8-n}W_{9+n}O_{47}$ $(1 \leq n \leq 6)$. Masters thesis, Universidad Autónoma de Nuevo León, School of Chemical Science **(1999)**.
21. K. Ishizuka and N. Uyeda, *Acta Crystallogr. A* 33, 740 **(1977)**.
22. F. L. Russell, J. K. Earl, and S. John, *Acta Crystallogr. A* 44, 912 **(1988)**.
23. *Jeol News* 34E (119), 16–19 **(1999)**.
24. CRISP (Crystallographic Electron Microscopy) Software, Versión 1.4a **(1996)**, Dr. George Farrantes, Calidris Manhemsvägen 4, 19145 Sollentuna, Sweden.
25. D. Garcia Gutierrez, C. Gutierrez Wing, M. Miki Yoshida, and M. J. Yacaman, *Appl. Phys. A* 79, 481 **(2004)**.
26. J. Taylor, T. Kippeny, and S. J. Rosenthal, *J. Clust. Sci.* 12, 571 **(2001)**.